

Unconventional ferromagnetic superexchange in CdVO_3 : The role of Cd

Alexander A. Tsirlin,^{*} Oleg Janson, and Helge Rosner[†]

Max Planck Institute for Chemical Physics of Solids, Nöthnitzer Str. 40, 01187 Dresden, Germany

A microscopic magnetic model of the low-pressure modification of CdVO_3 is established, based on density functional theory (DFT) band-structure calculations, magnetization measurements, and quantum Monte-Carlo simulations. This compound is a rare example of a quasi-one-dimensional spin- $\frac{1}{2}$ system showing exclusively ferromagnetic exchange. The spin lattice of CdVO_3 entails zigzag chains with an effective intrachain coupling $J \simeq -90$ K and interchain couplings of $J_c \simeq -18$ K and $J_a \simeq -3$ K. Quantum fluctuations are partially suppressed by the sizable interchain coupling J_c that leads to an intermediate regime between one-dimensional and two-dimensional ferromagnetic systems. Apart from the peculiar spin model, CdVO_3 features an unconventional mechanism of ferromagnetic superexchange. The couplings largely originate from Cd $5s$ states mediating hoppings between half-filled and empty orbitals of V^{+4} . The correct description of the ferromagnetic ground state in CdVO_3 is a challenge for DFT+ U methods that produce bewildering results for the exchange couplings in this compound.

PACS numbers: 75.30.Et, 75.10.Jm, 75.50.Gg, 71.20.Ps

I. INTRODUCTION

Ferromagnetism and antiferromagnetism, the two opponent magnetic interactions, are rarely balanced, because specific mechanisms of the magnetic exchange tend to favor one of the two options. For example, itinerant systems are prone to ferromagnetic Stoner instabilities, whereas superexchange in magnetic insulators is a source of mostly antiferromagnetic (AFM) interactions.¹ This makes AFM ground states more common among insulating transition-metal compounds. Antiferromagnetism utterly dominates in low-dimensional magnets, where long-range and typically AFM couplings between the low-dimensional units (chains or layers) induce the overall AFM order. In particular, most of the one-dimensional (1D) spin- $\frac{1}{2}$ ferromagnetic-chain systems are antiferromagnetically ordered because the interchain couplings are AFM.^{2–4} Low-dimensional spin- $\frac{1}{2}$ magnets with ferromagnetic (FM) ground state are still rare and restricted to systems based on organic radicals^{5,6} or Cu^{+2} compounds with non-trivial orbital ordering.^{7–9}

The aforementioned trend is violated by one peculiar compound, the low-pressure modification¹⁰ of CdVO_3 . Its 1D crystal structure (Fig. 1),¹¹ featuring zigzag chains of edge-sharing VO_5 pyramids, seemingly represents an archetypal AFM insulator with orbital degrees of freedom eliminated by the square-pyramidal coordination of V^{+4} . The interchain couplings are expected to be AFM because of their long-range nature. Moreover, the next-nearest-neighbor intrachain coupling J_2 between the corner-sharing vanadium pyramids should also be AFM, as in CaV_2O_5 and related compounds (see Sec. V and Table V).^{12–14} However, experimental data disprove these empirical arguments, and disclose FM order in CdVO_3 below $T_C = 24$ K.¹¹ Magnetic susceptibility was fitted with an expression for the classical spin- $\frac{1}{2}$ chain model to yield an effective intrachain coupling $J = -100$ K.¹¹ Dai *et al.*¹⁵ found $J_1 \simeq -288$ K and $J_2 \simeq -90$ K from generalized gradient approximation (GGA) band struc-

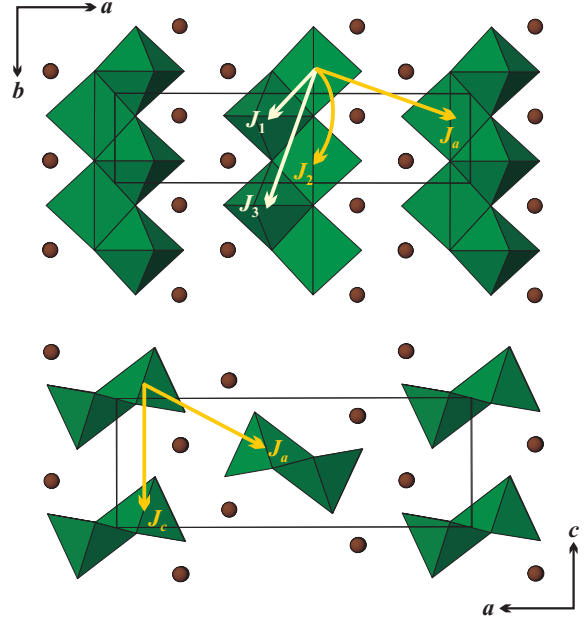


FIG. 1. (Color online) Crystal structure of CdVO_3 featuring zigzag chains of VO_5 pyramids. The chains are separated by Cd atoms (spheres).

ture calculations. They tentatively ascribed the unusual FM J_2 to the shift of the vanadium atom toward the base of the pyramid. However, their estimate of J_1 severely exceeds the experimental coupling of -100 K and, more importantly, does not address the nature of the interchain couplings, which are the driving force of the puzzling FM order in CdVO_3 .

In the following, we explore the microscopic mechanism of ferromagnetism in CdVO_3 by extensive band structure calculations combined with magnetization measurements and quantum Monte-Carlo (QMC) simulations. The application of diverse approaches for the evaluation of exchange couplings, along with the direct comparison to the

experimental data, leads to a reliable microscopic magnetic model of CdVO_3 . We show that the FM behavior of this compound is unconventional, and relate the ferromagnetism to Cd 5s orbitals mediating the FM superexchange. We also demonstrate instructive shortcomings of calculating exchange integrals with density functional theory (DFT)+ U methods. Below, the methodological part (Sec. II) is followed by band structure results in Sec. III and an analysis of the experimental data in Sec. IV. We conclude with a brief discussion and summary in Sec. V.

II. METHODS

The band structure was calculated within the framework of DFT using the full-potential local-orbital scheme (FPL08.50–32).¹⁶ We applied the local-density-approximation (LDA) with the Perdew-Wang parametrization¹⁷ for the exchange-correlation potential. Exchange couplings were evaluated via two different procedures, a model approach and a supercell approach. In the former, the LDA band structure was mapped onto a multi-orbital Hubbard model that was further treated perturbatively in the strongly correlated limit. In the supercell approach, the correlation effects in the V 3d shell were treated in a mean-field fashion by the LSDA+ U method. Total energies for a number of collinear spin configurations were mapped onto the classical Heisenberg model to yield individual exchange couplings. Since the supercell approach led to rather puzzling results, we performed an extensive cross-check using: i) GGA¹⁸ within FPL0; ii) Vienna *ab initio* simulation package (VASP)¹⁹ that performs projected augmented wave calculations and therefore employs a different basis set.^{20–22} LDA results were obtained for the orthorhombic crystallographic unit cell, with a fine k mesh of 1040 points in the symmetry-irreducible part of the first Brillouin zone. DFT+ U calculations utilized supercells doubled along b or c , with k meshes of 150 – 200 points.

To evaluate the magnetic susceptibility and Curie temperature of the proposed spin model, we performed QMC simulations using the `loop` algorithm²³ from the ALPS package.²⁴ 1D and two-dimensional (2D) finite lattices comprised $N = 120$ and 512 (32×16) sites, respectively, and ensured the absence of finite-size effects for the magnetic susceptibility within the temperature range under investigation. The Curie temperature was estimated from simulations for a three-dimensional (3D) model with different lattice sizes (see Sec. IV).

Experimental magnetization data were collected with a SQUID magnetometer (Quantum Design MPMS) in the temperature range 2 – 380 K in applied fields up to 5 T. The single-phase polycrystalline sample of CdVO_3 was prepared by a solid-state reaction of CdO and VO_2 in an evacuated silica tube at 700 °C for 24 hours. A 25 % excess of CdO was introduced to compensate for the losses caused by the volatilization and reaction with

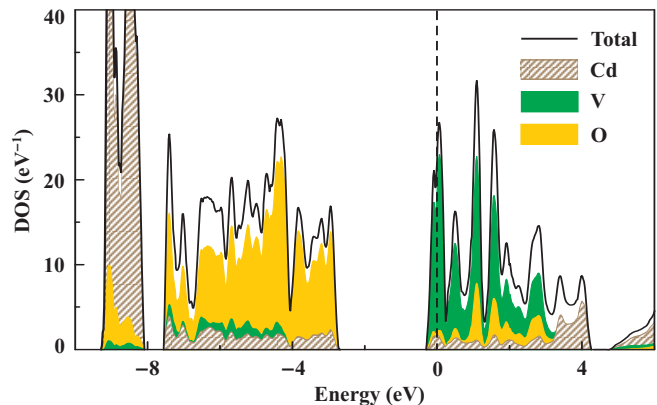


FIG. 2. (Color online) LDA density of states for CdVO_3 . The Fermi level is at zero energy.

the tube. The phase purity of the sample was checked by x-ray powder diffraction (Huber G670 Guinier camera, $\text{CuK}\alpha_1$ radiation, image-plate detector, $2\theta = 3 - 100^\circ$ angle range).

III. BAND STRUCTURE AND EXCHANGE COUPLINGS

A. LDA and model approach

The LDA band structure of CdVO_3 (Fig. 2), with oxygen 2p valence bands below -3 eV and vanadium 3d bands at the Fermi level (E_F), is reminiscent of other V^{+4} oxides.^{13,25} The contribution of cadmium is, however, larger than typical for an alkaline-earth (e.g., Ca^{+2} , Sr^{+2})^{13,25} or even a d^{10} (e.g., Ag^{+1} , Zn^{+2})^{26,27} cation. The bands below -8 eV originate from the filled Cd 4d orbitals, whereas the states at $3 - 4$ eV show predominantly Cd 5s character. It is worth to note that the contributions of Cd and O at the Fermi level are comparable, yet oxygen 2p states dominate over Cd 5s between 1 eV and 3 eV. The sizable contribution at E_F distinguishes Cd from other cations that also produce conduction bands $3 - 4$ eV above the Fermi level, but show a negligible contribution at E_F [for instance, Pb^{+2} in $\text{PbZnVO}(\text{PO}_4)_2$ (Ref. 27) or Se^{+4} in VOSeO_3 (Ref. 28)]. The obtained gapless energy spectrum originates from the underestimation of correlation effects in LDA. LSDA+ U reproduces a band gap of about 2.0 eV ($U_d = 4$ eV, FPL0) in reasonable agreement with the brown color of CdVO_3 .

The band complex between -0.5 eV and 4.2 eV comprises 24 bands (Fig. 3). Since there are four formula units per cell, these bands arise from six orbitals per formula unit: five V 3d and one Cd 5s. The 3d levels of vanadium lie below the Cd states, and show a crystal-field splitting characteristic of V^{+4}O_5 square pyramids.^{29,30} Directing the z axis along the short (apical) V–O bond of the VO_5 pyramid, we find the lowest-lying d_{xy} crystal-field level, represented by four narrow bands at the Fermi

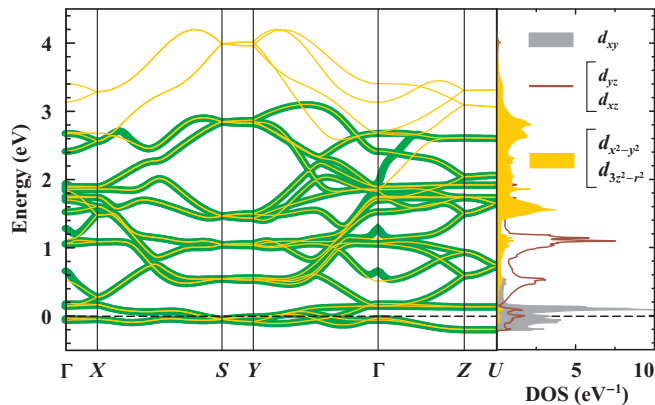


FIG. 3. (Color online) Left: LDA band structure for CdVO_3 (thin light lines) and the fit of the tight-binding model (thick dark lines) for the V $3d$ -related bands. Right: orbital-resolved DOS for V $3d$ states. The Fermi level is at zero energy. The poor fit in the vicinity of the Γ point is related to the strong hybridization with the Cd $5s$ states represented by the four high-lying bands (not fitted). The notation of k points is: $\Gamma(0, 0, 0)$, $X(0.5, 0, 0)$, $S(0.5, 0.5, 0)$, $Y(0, 0.5, 0)$, $Z(0, 0, 0.5)$, and $U(0.5, 0, 0.5)$.

level (Fig. 3).

To analyze exchange couplings, we fit 20 vanadium bands³¹ with a tight-binding model based on Wannier functions with proper orbital characters,³² and map the resulting transfer integrals t (hoppings) onto a multi-orbital Hubbard model with the effective on-site Coulomb repulsion $U_{\text{eff}} = 4$ eV and Hund's coupling $J_{\text{eff}} = 1$ eV.^{33,34} In the $t \ll U_{\text{eff}}$ limit, this model is reduced to the Kugel-Khomskii model, and the exchange couplings are expressed as follows:^{35,36}

$$J = \frac{4t_{xy}^2}{U_{\text{eff}}} - \sum_{\alpha} \frac{4t_{xy \rightarrow \alpha}^2 J_{\text{eff}}}{(U_{\text{eff}} + \Delta_{\alpha})(U_{\text{eff}} + \Delta_{\alpha} - J_{\text{eff}})}, \quad (1)$$

where t_{xy} and $t_{xy \rightarrow \alpha}$ are transfers between the xy states and from the xy (half-filled) to α (empty) states, respectively. Δ_{α} stands for the crystal-field splitting between the xy and α states. With Eq. (1), one evaluates full exchange couplings that are a sum of the AFM superexchange, arising from the transfers between the half-filled xy orbitals [Eq. (1), first term], and the FM superexchange due to the hoppings to empty d orbitals [Eq. (1), second term]. The efficiency of the LDA-based model approach has been demonstrated in Refs. 27, 33, and 34 providing a direct comparison to the experiment.

The leading exchange couplings calculated according to Eq. (1) are listed in Table I. The FM components of J_1 and J_2 surpass the AFM superexchange. The inter-chain coupling along c lacks any AFM component, yet there is a sizable FM contribution of -17 K. The inter-chain coupling along a is weaker but also FM. Further couplings are below 2 K (in terms of the absolute value) with an exception of $J_3 \simeq -8$ K, which is the third-neighbor intrachain coupling.

TABLE I. Interatomic distances (in \AA) in the CdVO_3 structure and the exchange couplings (in K) calculated with Eq. (1): the AFM (J^{AFM}) and FM (J^{FM}) contributions and the resulting total exchange (J).

| | Distance | J^{AFM} | J^{FM} | J |
|-------|----------|------------------|-----------------|-----|
| J_1 | 3.05 | 18 | -87 | -69 |
| J_2 | 3.60 | 21 | -30 | -9 |
| J_3 | 5.93 | 0 | -8 | -8 |
| J_c | 5.20 | 0 | -17 | -17 |
| J_a | 5.79 | 1 | -4 | -3 |

The exclusively FM couplings in CdVO_3 readily lead to the FM long-range order. Therefore, the results of the model approach are qualitatively consistent with the experimental data. A further, and quantitative, comparison is given in Sec. IV. In the rest of the present section, we focus on the supercell approach that fails to produce an unambiguous FM scenario (Sec. III B), and find out the microscopic origin of ferromagnetism in CdVO_3 (Sec. III D).

B. DFT+ U puzzles

The supercell approach to the evaluation of exchange couplings is based on mean-field LSDA+ U (more generally, DFT+ U) calculations that are sensitive to: i) the choice of the on-site Coulomb repulsion (U_d) and exchange (J_d) parameters; ii) the choice of the double-counting correction (DCC) scheme, around-mean-field (AMF) or fully-localized-limit (FLL). In general, both choices are made on empirical grounds, and by far are not unambiguous. Here, we focus on the effect of DCC, with U_d and J_d fixed at 3 eV and 1 eV, respectively. The aforementioned values have been justified by FPL0 LSDA+ U calculations for several V^{4+} compounds.^{29,33,34} We also varied U_d in the physically reasonable range of 2.5–6 eV, but no qualitative differences were found. To avoid calculations for large supercells, we estimated $J_1 + J_3$ instead of evaluating J_1 and J_3 separately. According to Table I, $|J_3| \ll |J_1|$, i.e., one may assume $J_1 + J_3 \simeq J_1$.

The AMF and FLL results for the exchange couplings in CdVO_3 are completely different (Table II). While AMF describes CdVO_3 as a mostly AFM system with a single FM coupling J_1 , FLL suggests a predominantly FM scenario with a single AFM coupling J_2 . Essentially the same results are obtained in GGA+ U . VASP calculations can be done for FLL only, and support the respective results from FPL0. Note that we used a higher U_d of 4 eV to reproduce a typical 1 eV offset related to different basis sets in VASP and FPL0.^{22,37} Another remark regards the GGA (without U) results by Dai *et al.*¹⁵ who found both J_1 and J_2 FM, with a clearly overestimated absolute value of J_1 . Their results cannot be directly compared to ours, because uncorrelated GGA calculations heavily un-

TABLE II. Exchange couplings (in K) evaluated by the DFT+ U supercell procedure for different functionals, double-counting-correction (DCC) schemes, and band structure codes. The DFT+ U parameters are set to $U_d = 3$ eV (FPL0), $U_d = 4$ eV (VASP), and $J_d = 1$ eV (both codes).

| $J_1 + J_3$ | J_2 | J_a | J_c | Functional | DCC | Code |
|-------------|-------|-------|-------|------------|-----|------|
| -17 | 21 | 2 | 9 | LSDA+ U | AMF | FPL0 |
| -18 | 30 | 2 | 8 | GGA+ U | AMF | FPL0 |
| -130 | 11 | -4 | -24 | LSDA+ U | FLL | FPL0 |
| -117 | 17 | -3 | -17 | GGA+ U | FLL | FPL0 |
| -122 | -4 | -3 | -26 | LSDA+ U | FLL | VASP |

derestimate correlation effects (for example, the reported band gap of about 0.5 eV¹⁵ is much too small to explain the brown color of CdVO₃). The neglect of strong correlation effects typically leads to huge errors in the exchange couplings, as demonstrated in, e.g., Ref. 38.

A simple qualitative analysis shows that the FLL results are in agreement with the experiment, whereas the AMF results are obviously wrong. To achieve the FM ground state, the interchain couplings J_a and J_c should be FM. The AFM next-nearest-neighbor intrachain coupling J_2 frustrates J_1 , yet it does not break the FM ground state at $J_2/|J_1| < \frac{1}{4}$ (Ref. 39). The FLL results $J_a, J_c < 0$ and $J_2/|J_1| \leq 0.15$ fulfill both conditions. By contrast, $J_2/|J_1| \simeq 1$ obtained in AMF induces a spiral order along the chains that are further coupled antiferromagnetically. Therefore, the AMF-based scenario is unrealistic.

Seemingly, the above analysis puts forward the advantages of FLL in evaluating the exchange couplings. This conclusion is reinforced by the physical meaning of different DCC schemes.⁴⁰ While AMF describes the regime of moderate correlations, FLL should be appropriate for strongly correlated systems ($t_i \ll U_{\text{eff}}$), such as CdVO₃. However, the available AMF results for a number of V⁺⁴ compound tip the scales and make the situation less clear. In Refs. 26, 33, and 34, we have shown that AMF leads to remarkably good agreement with the experiment for vanadium oxides. Moreover, AMF shows better performance for many cuprates.^{37,41} In the following, we perform a further test to establish empirical criteria regarding the influence of the DCC scheme on the exchange couplings in V⁺⁴ compounds.

C. Double-counting correction: AMF vs. FLL

To compare the performance of the AMF and FLL versions of DFT+ U , we select five representative V⁺⁴ compounds showing chain-like magnetic behavior (Table III). While details of the interchain couplings and the magnetic ground state may be different (and, in some cases, not fully understood), the AFM nature of the intrachain

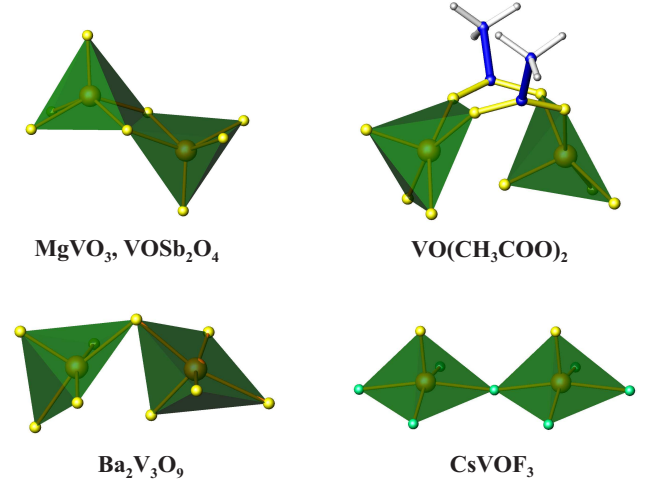


FIG. 4. (Color online) Superexchange pathways in test compounds listed in Table III.

couplings is safely established experimentally.^{25,42–45} The key difference between our test systems is the mutual arrangement of the vanadium polyhedra. To analyze the connectivity, we only consider the magnetic unit, a VO₅ square pyramid, despite the actual crystallographic local environment is often described as an octahedron. The advantage of our description is the simple identification of the relevant superexchange pathway through oxygen atoms lying in the basal plane of the pyramid. Since all systems under consideration reveal the d_{xy} orbital ground state, the axial oxygen atom neither connects the pyramids nor contributes to the superexchange.

The test systems represent several different regimes (Fig. 4): i) edge-sharing VO₅ pyramids (VOSb₂O₄, the low-pressure modification of MgVO₃);^{42,43} ii) corner-sharing VO₅ pyramids with either twisted (Ba₂V₃O₉, V–O–V angle of 96.4°)²⁵ or nearly linear (CsVOF₃, V–O–V angle of 164.9°)⁴⁴ geometries; iii) VO₅ pyramids bridged by a non-magnetic acetate (CH₃COO[−]) group.⁴⁵

The intrachain exchange coupling J is evaluated as the energy difference between the FM and AFM spin configurations. Further couplings, both interchain and long-range intrachain, are rather weak and irrelevant for the present analysis. Quantitative estimates of these weak couplings and detailed structural information can be found in the preceding studies.^{25,46–48}

In Table III, we compare AMF and FLL results for the leading intrachain exchange couplings. The corner-sharing (Ba₂V₃O₉, CsVOF₃) or indirect [VO(CH₃COO)₂] connections between the VO₅ pyramids lead to a remarkably small difference between AMF and FLL. By contrast, there are large discrepancies for the couplings between edge-sharing pyramids, especially in MgVO₃. These discrepancies are basically independent of the U_d value, because J^{AMF} and J^{FLL} show similar evolution with a nearly constant offset of $J^{\text{AMF}} - J^{\text{FLL}} \simeq 100$ K in VOSb₂O₄ and about 200 K in MgVO₃ (Fig. 5).

TABLE III. Test quasi-1D V^{+4} compounds, the V–V distances d (in Å), the connections between the VO_5 pyramids, and the exchange couplings J (in K) obtained from the AMF or FLL supercell calculations⁴⁹ and from the experiment.

| Compound | $d(V-V)$ | Connection | J^{AMF} | J^{FLL} | J^{exp} | Ref. |
|---|----------|---------------------|-----------|-----------|-----------|------|
| MgVO ₃ | 2.98 | edge-sharing | 128 | −84 | 100 | 42 |
| VOSb ₂ O ₄ | 3.01 | edge-sharing | 248 | 154 | 250 | 43 |
| Ba ₂ V ₃ O ₉ | 3.01 | corner-sharing | 79 | 84 | 94 | 25 |
| CsVOF ₃ | 3.91 | corner-sharing | 143 | 157 | 132 | 44 |
| VO(CH ₃ COO) ₂ | 3.48 | via acetate bridges | 544 | 528 | 430 | 45 |

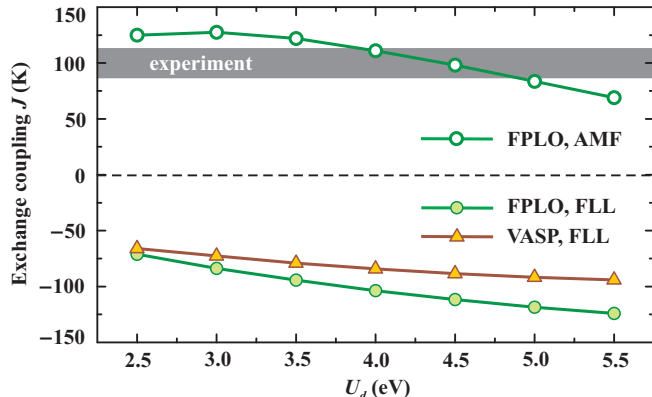


FIG. 5. (Color online) Intrachain exchange coupling in MgVO₃ calculated by LSDA+ U for different values of Coulomb repulsion parameter U_d and different DCC schemes: AMF (open symbols) and FLL (filled symbols). The marginal difference between the FLL results obtained in FPLO and in VASP is likely related to different basis sets.⁵⁰

In VOSb₂O₄, the discrepancy might be still tolerable, because both types of DCC yield the correct antiferromagnetic solution. The weaker exchange coupling, along with a larger offset between AMF and FLL, make the FLL result for MgVO₃ qualitatively wrong. Fig. 5 shows that any reasonable value of U_d leads to negative J^{FLL} violating the experimental AFM coupling. The VASP calculations for MgVO₃ produce similar J values and confirm the intrinsic nature of the problem.

Based on our findings for test compounds, we arrive at two empirical conclusions: i) substantial differences between AMF and FLL are found for short V–V separations and, specifically, edge-sharing VO_5 pyramids only; ii) for edge-sharing pyramids, neither DCC can be used reliably. The results from AMF are in good agreement with the experiment for MgVO₃ and VOSb₂O₄, but qualitatively wrong for CdVO₃. The FLL results are qualitatively wrong for MgVO₃, yet rather accurate for CdVO₃. Previous computational studies of V^{+4} oxides^{33,34} showed consistent AMF and FLL results for long-range couplings, thus confirming our first conclusion. We argue that DFT+ U calculations can be safely used for systems lacking the edge-sharing connections between the VO_5

pyramids. However, short V–V distances cause an apparent problem which deserves further investigation.

D. Origin of ferromagnetism

The FM behavior of CdVO₃ contrasts with the AFM properties of other V^{+4} compounds, such as quasi-1D MgVO₃ and VOSb₂O₄ or quasi-2D CaV₂O₅, CaV₃O₇, and CaV₄O₉. While J_1 is a nearly 90° and possibly FM V–O–V superexchange, the weakness of J_2 as well as the FM nature of J_a and J_c are less clear from a microscopic point of view. Dai *et al.*¹⁵ claimed that the shift of the vanadium atom toward the basal plane of the VO_5 pyramid could cause FM J_2 . However, they did not verify this conjecture, and refrained from any analysis of the FM interchain couplings, which are crucial for the FM long-range order. Here, we argue that the origin of ferromagnetism in CdVO₃ is different, and relates to the admixture of Cd states to the magnetic orbitals (Wannier functions). We justify this mechanism by considering a model system, a hypothetical CaVO₃ compound with the atomic structure of CdVO₃ and Ca occupying the Cd position. In our analysis, we follow the approach of Refs. 13, 27, and 29 that utilize the ability of DFT to evaluate microscopic parameters of fictitious compounds and, therefore, investigate the influence of different structural features on the magnetic properties.

The band structures of CdVO₃ and hypothetical CaVO₃ are rather similar, yet CaVO₃ is free from the low-lying Cd 5s bands (compare Figs. 2 and 6). Therefore, vanadium bands are largely mixing with O 2p and basically lack the cation contribution. This change in the band structure has a strong effect on individual transfer integrals and the resulting exchange couplings (Table IV). Compared to Table I, the main differences in the results of the model analysis are: i) the increase in AFM J_2 ; ii) the AFM nature of J_a and J_c ; iii) isotropic interchain couplings ($J_a \simeq J_c$). The hypothetical CaVO₃ is predicted to be predominantly antiferromagnetic, and conforms to the trends established for V^{+4} compounds. Specifically, the long-range interchain couplings are AFM, whereas J_2 is about 100 K, as in MgV₂O₅ and CaV₄O₉ (see Sec. V and Table V).

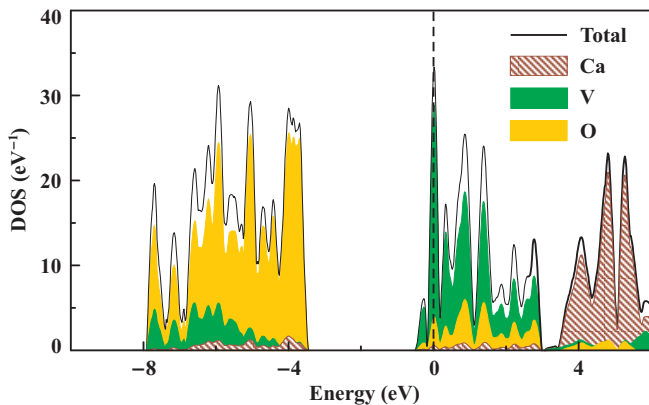


FIG. 6. (Color online) LDA density of states for the fictitious CdVO_3 -type CaVO_3 (compare to Fig. 2). The Fermi level is at zero energy.

TABLE IV. Exchange couplings (in K) in the hypothetical CaVO_3 compound with the CdVO_3 structure. The J^{AFM} , J^{FM} , and $J = J^{\text{AFM}} + J^{\text{FM}}$ values are obtained from Eq. (1) (model approach), whereas the numbers in the last two columns (AMF and FLL) are calculated via the supercell approach with different DCC (LSDA+ U , $U_d = 3$ eV, $J_d = 1$ eV). Similar to Table II, the LSDA+ U estimates of J_1 are in fact $J_1 + J_3$ with $J_3 \simeq 5$ K according to the model analysis.

| | J^{AFM} | J^{FM} | J | J | J |
|-------|------------------|-----------------|-----|-----|------|
| | Model approach | | | AMF | FLL |
| J_1 | 26 | -42 | -16 | -28 | -163 |
| J_2 | 105 | -23 | 82 | 133 | 83 |
| J_c | 0.3 | 0 | 0.3 | 1 | -3 |
| J_a | 1.2 | -1.1 | 0.1 | 2 | -2 |

The LSDA+ U results for CaVO_3 reveal the same problems as in CdVO_3 (compare Tables II and IV). The AMF and FLL calculations basically agree on the sizable AFM J_2 , but strikingly differ in the estimate of FM J_1 . Additionally, AMF and FLL systematically predict positive and negative interchain couplings, respectively. The AMF results are now in reasonable agreement with the model approach, while the FLL estimates are qualitatively different. Both AMF and FLL partly reproduce the changes induced by the Cd orbitals: irrespective of the computational method, we find a clear reduction in J_2 and the increase in the absolute values of J_c upon going from CaVO_3 to CdVO_3 , yet J_1 is basically unchanged. We also note the general tendency of FLL to overestimate FM contributions (also for the weak interchain couplings). Based on this analysis, we conclude that the remarkable performance of FLL for CdVO_3 is, at least partly, a matter of coincidence: the overestimated FM couplings casually match the actual ferromagnetism of the compound. In other V^{+4} oxides, the AMF results are usually in better agreement with the model approach

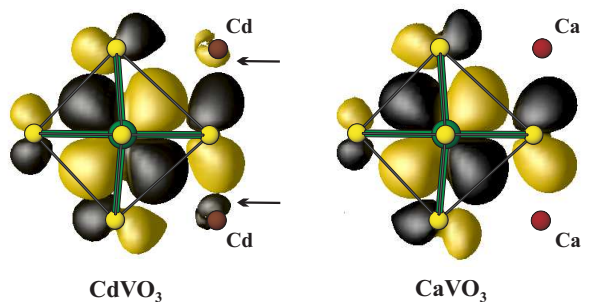


FIG. 7. (Color online) Vanadium d_{xy} -based Wannier functions for CdVO_3 (left) and hypothetical CaVO_3 (right). Note the Cd 5s contributions (marked with arrows) that are missing in the Ca-containing compound.

and experiment (Table III).

The role of the Cd 5s states in the magnetism of CdVO_3 is further evidenced by Wannier functions. In Fig. 7, we compare the V d_{xy} -based Wannier functions for CdVO_3 and CaVO_3 . Apart from the leading V d_{xy} contributions, both Wannier functions comprise oxygen p orbitals. In CdVO_3 , there is an additional Cd 5s contribution, which is missing in CaVO_3 . Similar features are found for Wannier functions based on empty vanadium orbitals. The Cd orbitals represent “tails” of the Wannier functions and amplify interorbital hoppings that drive the FM superexchange.

IV. ANALYSIS OF THE EXPERIMENTAL DATA

The magnetic susceptibility (χ) of CdVO_3 steeply increases from 380 K to 2 K and clearly indicates the FM nature of the system (Fig. 8). At low temperatures, the magnetization reaches the saturated value of about $1 \mu_B$ at the applied field of less than 0.2 T. The lack of hysteresis may be related to a very weak anisotropy of V^{+4} (Ref. 51). Above 230 K, the susceptibility follows the Curie-Weiss law

$$\chi = \chi_0 + \frac{C}{T + \theta}, \quad (2)$$

where $\chi_0 = -70 \times 10^{-6}$ emu/mol is the temperature-independent contribution of core diamagnetism and van Vleck paramagnetism, $C = 0.368$ emu K mol $^{-1}$ is the Curie constant, and $\theta = -46$ K is the Weiss temperature. The C value corresponds to the effective magnetic moment of $1.70 \mu_B$ that perfectly matches the expected value of $g\mu_B\sqrt{S(S+1)} = 1.697 \mu_B$ with $g = 1.96$ from ESR.¹¹ The negative Weiss temperature is a signature of FM couplings leading to a positive deviation from the Curie-Weiss behavior below 230 K.

Onoda and Nishiguchi¹¹ fitted the magnetic suscepti-

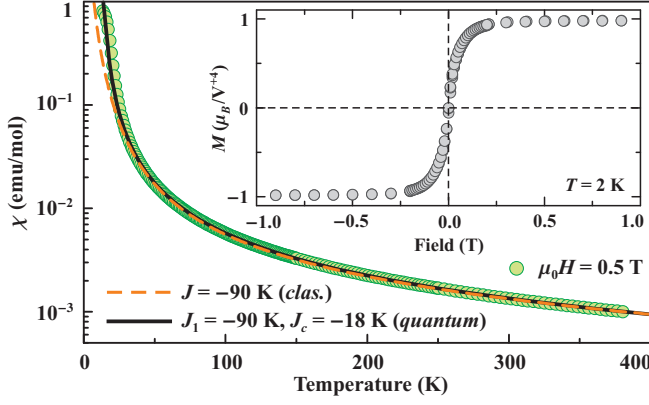


FIG. 8. (Color online) Magnetic susceptibility of CdVO_3 measured in an applied field of 0.5 T (filled circles) and the fits with the classical 1D model (dashed line) as well as the quantum 2D $J_1 - J_c$ model (solid line). Inset: magnetization curve at 2 K.

bility with the expression for the classical spin- $\frac{1}{2}$ chain:⁵²

$$\chi = \chi_0 + \frac{N_A g^2 \mu_B^2}{4k_B T} \frac{1+u}{1-u}, \quad u = \coth\left(-\frac{3J}{4T}\right) + \frac{4T}{3J}. \quad (3)$$

Our data can be described in a similar way ($\chi_0 = -70 \times 10^{-6}$ emu/mol, $g = 1.99$, $J = -90$ K, dashed line in Fig. 8), but the model itself does not apply to the spin- $\frac{1}{2}$ compound CdVO_3 because of inherent quantum fluctuations in low-dimensional spin- $\frac{1}{2}$ systems. For example, the classical AFM spin- $\frac{1}{2}$ chain shows the susceptibility maximum at $T_{\text{max}}/J \simeq 0.35$, whereas for the quantum AFM chain $T_{\text{max}}/J \simeq 0.64$. A pronounced difference should also be expected for the FM case. Indeed, the simulated curve for the quantum FM chain ($J = -120$ K) fits our experimental data down to 100 K only (short-dashed line in Fig. 9). At lower temperatures, the 1D quantum model underestimates the susceptibility. This should be understood as an effect of quantum fluctuations that disturb the parallel alignment of spins and therefore reduce χ .

Since the experimental data for CdVO_3 conform to the classical model (see Fig. 8), quantum fluctuations in this compound are less pronounced than in the single quantum spin chain. This reduction could be related to the interchain coupling J_c that increases the dimensionality, or the FM intrachain coupling J_2 that increases the number of bonds at a lattice site without changing the dimensionality. We start with the first option, which is also favored by DFT since $|J_2| \ll |J_1|$. The 2D $J_1 - J_c$ model fits the experimental data down to 30 K with $J_1 = -90$ K, $J_c/J_1 = 0.2$, $g = 1.96$, and $\chi_0 = -80 \times 10^{-6}$ emu/mol (solid line in Fig. 9). For comparison, we also considered the isotropic 2D model (FM square lattice, $J_c = J_1 = -50$ K) where quantum fluctuations are further suppressed by the increased dimensionality. This model consequently overestimates the susceptibility below 90 K (dash-dotted line in the

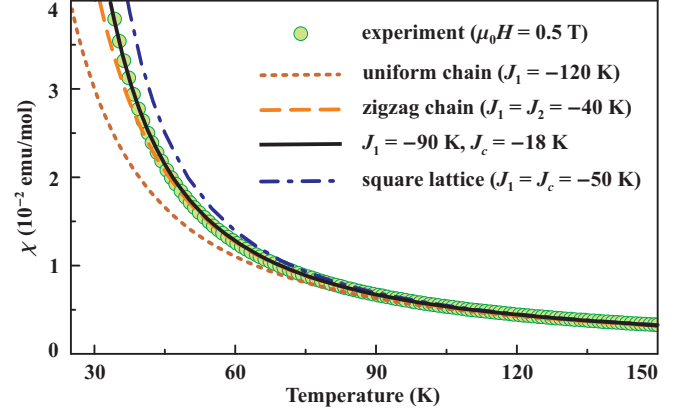


FIG. 9. (Color online) Fits of the magnetic susceptibility with different 1D and 2D spin models, see text for details.

same figure). Therefore, CdVO_3 exhibits an intermediate regime between 1D and 2D FM systems.

The long-range FM order in CdVO_3 is stabilized by the interchain couplings J_a and J_c . To evaluate the Curie temperature T_C , we considered the 3D $J_1 - J_c - J_a$ spin model and calculated the Binder ratio of magnetization $B(T) = \langle m^2 \rangle / \langle m \rangle^2$ for finite lattices of different size. The Curie temperature was determined as the crossing point of several $B(T)$ curves calculated for $L \times L/2 \times L/2$ finite lattices with $L \leq 64$. Similar to Refs. 53 and 54, we reduced the dimensions of the lattices along J_a and J_c to account for the anisotropic nature of our system. Using $J_a/J_1 = 0.03$ (Tables I and II), we arrive at $T_C/J_1 = 0.212$ ($T_C = 19$ K) that is slightly below the experimental value of 24 K.⁵⁰

The marginal underestimate of T_C in the $J_1 - J_a - J_c$ model may be related to magnetic anisotropy, which lies beyond the scope of the present study, or the second-neighbor intrachain coupling J_2 . According to DFT results, this coupling is either weakly FM (Table I) or weakly AFM (Table II). The AFM J_2 introduces frustration and disables the QMC techniques because of the sign problem. By contrast, the effect of FM J_2 can be readily evaluated. At weak FM J_2 , the overall energy of the intrachain exchange (-90 K) is merely redistributed between J_1 and J_2 . Using $J_1 = J_2 = -40$ K, we are able to introduce more significant changes by reducing quantum fluctuations and improving the susceptibility fit even within the purely 1D $J_1 - J_2$ model (long-dashed line in Fig. 9). The second-neighbor coupling J_2 brings the system closer to the classical regime, thereby reducing the fitted interchain coupling. Since the ordering temperature is mostly sensitive to the value of J_c , the $J_1 - J_2 - J_a - J_c$ model further underestimates T_C . Therefore, the sizable FM J_2 is unlikely. In conclusion, we argue that the unfrustrated $J_1 - J_a - J_c$ spin lattice, providing a remarkable fit of the susceptibility and a reasonable estimate of T_C , is a valid microscopic model of CdVO_3 supporting our DFT results. Further effects should likely be ascribed to the magnetic anisotropy.

V. DISCUSSION AND SUMMARY

The unconventional ferromagnetism of CdVO_3 puts forward several important issues. First, we have demonstrated the difficulties in calculating exchange integrals for this compound. While the model approach produces reasonable estimates of J_i , the DFT+ U calculations lead to bewildering results that are strongly dependent on the double-counting correction. Although we are presently unable to unravel the origin of these problems, systematic calculations for V^{+4} compounds confine the ambiguity of DFT+ U to short-range couplings between edge-sharing VO_5 pyramids (Table III). The long-range couplings are basically unaffected by the DCC and compare well to the results of the model analysis. For short-range couplings, the model estimates are also robust, while the DFT+ U estimates should be taken with caution.

Recent computational studies of Cu^{+2} compounds revealed similar problems of the supercell approach applied to short-range couplings.^{37,41} The case of cuprates is, however, less formidable because the differences between the AMF and FLL results are largely balanced by the proper choice of the U_d parameter.^{37,55,56} In V^{+4} compounds, the adjustment of U_d does not resolve the problem, as demonstrated by the instructive example of MgVO_3 (Fig. 5). The sheer amount of observations regarding the influence of DCC on the DFT+ U results calls for a further investigation of this matter. The short-range couplings in V^{+4} oxides may also be appropriate for testing alternative computational approaches to exchange couplings in strongly correlated electronic systems.

The unexpected FM behavior of CdVO_3 originates from Cd 5s states mediating the hoppings between the half-filled and empty orbitals of V^{+4} . The interaction is, therefore, a sort of superexchange, but its mechanism is different from the conventional orbital ordering scenario.^{8,35} The orbital ordering induces magnetic (half-filled) orbitals of different symmetry on the neighboring atoms, and favors the hoppings between the half-filled and empty orbitals of the same symmetry. In CdVO_3 , there is only one type of the magnetic orbital, hence ferromagnetism is driven by hoppings between orbitals of different symmetry.

The effect of Cd is easily recognized in Table V that compares exchange couplings between the corner-sharing VO_5 pyramids. Although one generally expects the increase in the AFM superexchange at V–O–V angles close to 180° , this trend does not hold for V^{+4} compounds due to the relevance of other structural features. For example, basal planes of the pyramids coincide in CaV_2O_5 and CsVOF_3 , but remain nearly perpendicular in $\text{Ba}_2\text{V}_3\text{O}_9$ (Fig. 4). This explains the broad range of possible V–O–V angles and their weak effect on the superexchange. The only general trend is the AFM nature of the coupling between the corner-sharing VO_5 pyramids. The couplings typically range between 100 and 200 K, and always exceed 90 K. CdVO_3 is a remarkable exception, with the AFM coupling reduced below 20 K because of the Cd 5s

TABLE V. Exchange couplings between corner-sharing VO_5 pyramids: V–O–V angles (in deg), V–V distances (in Å), and exchange couplings J (in K) estimated from the experiment (marked with an asterisk) or DFT calculations.

| Compound | $\alpha(\text{V-O-V})$ | $d(\text{V-V})$ | J | Ref. |
|-----------------------------------|------------------------|-----------------|------|-----------|
| $\text{Ba}_2\text{V}_3\text{O}_9$ | 96.4 | 3.01 | 94* | 25 |
| MgV_2O_5 | 117.6 | 3.37 | 92 | |
| | 141.1 | 3.69 | 144 | 12 |
| CaV_4O_9 | 129.9 | 3.54 | 148 | 12 |
| CaV_2O_5 | 132.9 | 3.49 | 608 | |
| | 135.3 | 3.60 | 122 | 12 |
| CdVO_3 | 136.1 | 3.60 | < 20 | This work |
| PbVO_3 | 147.7 | 3.80 | 203* | 26 |
| CsVOF_3 | 164.9 | 3.91 | 132* | 44 |

orbitals altering the superexchange.

The cation-mediated superexchange in vanadium oxides is not restricted to CdVO_3 . For example, the unusually strong and frustrating second-neighbor exchange in PbVO_3 is likely driven by Pb 6p orbitals that marginally contribute to the V d_{xy} bands.^{38,57} A similar “diagonal” superexchange has been proposed for $\text{Pb}_{0.55}\text{Cd}_{0.45}\text{V}_2\text{O}_5$, although the intrinsic disorder of Pb and Cd atoms in this compound hampered an accurate experimental estimate of the respective coupling.⁵⁸ The aforementioned systems are, however, different from CdVO_3 , and show AFM superexchange. We conclude that non-magnetic cations may have diverse effects on the superexchange, and the specific scenario is actually determined by the hybridization between the cation orbitals and oxygen orbitals entering vanadium-based Wannier functions. In many systems (e.g., vanadium phosphates²⁹), there is no effect at all because the cation states are expelled from the Fermi level. The cation-mediated superexchange is not ubiquitous and requires specific coupling geometries, but it can be expected for a variety of cations featuring empty s (e.g., Zn^{+2} , Cu^{+1} , Ag^{+1}) or p (e.g., Bi^{+3} , Sn^{+2}) states closely above the Fermi level (see also Ref. 59). Respective compounds are likely to host non-trivial spin lattices and unusual magnetism.

Finally, we note that CdVO_3 is interesting on its own as a system showing an intermediate regime between the 1D and 2D ferromagnets. Experimental studies of FM uniform chains helped to find appropriate theoretical tools for solving the Heisenberg model in 1D, and disclosed peculiar soliton-type excitations.^{60,61} The respective systems are close to the 1D limit, whereas the opposite, 2D limit is realized in K_2CuF_4 and related Cu^{+2} halides with layered perovskite-type structures.^{7–9} CdVO_3 could be a reference point between these two qualitatively different model regimes representing the ground states with zero (1D) and non-zero (2D) ordered magnetic moment. The crossover between the 1D and 2D regimes is rather well studied for the AFM case,⁵³ yet a

comparative study of the FM case could be insightful.

In summary, we have developed a microscopic magnetic model of CdVO_3 , and found out the origin of ferromagnetism in this compound. We argue that CdVO_3 is a ferromagnetic spin chain system with an effective (and mostly nearest-neighbor) intrachain coupling of -90 K and a sizable interchain coupling $J_c = -18$ K along one of the dimensions. Our model is based on extensive band structure calculations and verified by a direct comparison to the experimental magnetic susceptibility and Curie temperature. The unusual ferromagnetic couplings arise from Cd $5s$ orbitals that contribute to the vanadium-based Wannier functions, mediate hoppings between the

half-filled and empty orbitals of vanadium, and lead to the ferromagnetic superexchange. This mechanism puts forward diverse effects of non-magnetic cations on superexchange in transition-metal compounds.

ACKNOWLEDGMENTS

We are grateful to Yurii Prots and Horst Borrmann for x-ray diffraction measurements. A.T. was supported by Alexander von Humboldt foundation.

* altsirlin@gmail.com

† Helge.Rosner@cpfs.mpg.de

¹ P. W. Anderson, *Solid State Physics*, **14**, 99 (1963).

² C. P. Landee and R. D. Willett, *Phys. Rev. Lett.*, **43**, 463 (1979); C. Dupas, J. P. Renard, J. Seiden, and A. Cheikh-Rouhou, *Phys. Rev. B*, **25**, 3261 (1982).

³ D. D. Swank, C. P. Landee, and R. D. Willett, *Phys. Rev. B*, **20**, 2154 (1979).

⁴ R. D. Willett, C. P. Landee, R. M. Gaura, D. D. Swank, H. A. Groenendijk, and A. J. van Duynveldt, *J. Magn. Magn. Mater.*, **15-18**, 1055 (1980); R. Hoogerbeets, E. H. A. Bakr, and A. J. V. Duynveldt, *Physica B*, **128**, 161 (1985).

⁵ M. Takahashi, P. Turek, Y. Nakazawa, M. Tamura, K. Nozawa, D. Shiomi, M. Ishikawa, and M. Kinoshita, *Phys. Rev. Lett.*, **67**, 746 (1991); Y. Nakazawa, M. Tamura, N. Shirakawa, D. Shiomi, M. Takahashi, M. Kinoshita, and M. Ishikawa, *Phys. Rev. B*, **46**, 8906 (1992).

⁶ K. Shimizu, T. Gotohda, T. Matsushita, N. Wada, W. Fujita, K. Awaga, Y. Saiga, and D. S. Hirashima, *Phys. Rev. B*, **74**, 172413 (2006).

⁷ I. Yamada, *J. Phys. Soc. Jpn.*, **33**, 979 (1972); Y. Ito and J. Akimitsu, *ibid.*, **40**, 1333 (1976).

⁸ D. I. Khomskii and K. I. Kugel, *Solid State Comm.*, **13**, 763 (1973).

⁹ L. J. de Jongh, *Physica*, **82**, 247 (1976); R. Willett, H. Place, and M. Middleton, *J. Amer. Chem. Soc.*, **110**, 8639 (1988), and references therein.

¹⁰ Throughout the paper, we refer to the low-pressure modification of CdVO_3 . The high-pressure phase has a perovskite-type structure and exhibits metallic behavior [B. L. Chamberland and P. S. Danielson, *J. Solid State Chem.*, **10**, 249 (1974)].

¹¹ M. Onoda and N. Nishiguchi, *J. Phys.: Cond. Matter*, **11**, 749 (1999).

¹² M. A. Korotin, I. S. Elfimov, V. I. Anisimov, M. Troyer, and D. I. Khomskii, *Phys. Rev. Lett.*, **83**, 1387 (1999), cond-mat/9901214.

¹³ M. A. Korotin, V. I. Anisimov, T. Saha-Dasgupta, and I. Dasgupta, *J. Phys.: Cond. Matter*, **12**, 113 (2000), cond-mat/9907479.

¹⁴ W. E. Pickett, *Phys. Rev. Lett.*, **79**, 1746 (1997), cond-mat/9704203.

¹⁵ D. Dai, H.-J. Koo, and M.-H. Whangbo, *J. Solid State Chem.*, **175**, 341 (2003).

¹⁶ K. Koepf and H. Eschrig, *Phys. Rev. B*, **59**, 1743 (1999).

¹⁷ J. P. Perdew and Y. Wang, *Phys. Rev. B*, **45**, 13244 (1992).

¹⁸ J. P. Perdew, K. Burke, and M. Ernzerhof, *Phys. Rev. Lett.*, **77**, 3865 (1996).

¹⁹ G. Kresse and J. Furthmüller, *Comput. Mater. Sci.*, **6**, 15 (1996); *Phys. Rev. B*, **54**, 11169 (1996).

²⁰ P. E. Blöchl, *Phys. Rev. B*, **50**, 17953 (1994); G. Kresse and D. Joubert, *Phys. Rev. B*, **59**, 1758 (1999).

²¹ The energy cutoff was set to 400 eV.

²² The different basis sets in **FPLM** and **VASP** imply different implementation of the correlated $3d$ orbitals and, consequently, require an adjustment of input parameters for the DFT+ U scheme.

²³ S. Todo and K. Kato, *Phys. Rev. Lett.*, **87**, 047203 (2001), cond-mat/9911047.

²⁴ A. Albuquerque, F. Alet, P. Corboz, P. Dayal, A. Feiguin, S. Fuchs, L. Gamper, E. Gull, S. Gürtler, A. Honecker, R. Igarashi, M. Körner, A. Kozhevnikov, A. Läuchli, S. R. Manmana, M. Matsumoto, I. P. McCulloch, F. Michel, R. M. Noack, G. Pawłowski, L. Pollet, T. Pruschke, U. Schollwöck, S. Todo, S. Trebst, M. Troyer, P. Werner, and S. Wessel, *J. Magn. Magn. Mater.*, **310**, 1187 (2007).

²⁵ E. E. Kaul, H. Rosner, V. Yushankhai, J. Sichelschmidt, R. V. Shpanchenko, and C. Geibel, *Phys. Rev. B*, **67**, 174417 (2003), cond-mat/0209409.

²⁶ A. A. Tsirlin, R. Nath, C. Geibel, and H. Rosner, *Phys. Rev. B*, **77**, 104436 (2008), arXiv:0802.2293.

²⁷ A. A. Tsirlin, R. Nath, A. M. Abakumov, R. V. Shpanchenko, C. Geibel, and H. Rosner, *Phys. Rev. B*, **81**, 174424 (2010), arXiv:0910.2258.

²⁸ S.-H. Kim, P. S. Halasyamani, B. C. Melot, R. Seshadri, M. A. Green, A. S. Sefat, and D. Mandrus, *Chem. Mater.*, **22**, 5074 (2010).

²⁹ A. A. Tsirlin and H. Rosner, *Phys. Rev. B*, **79**, 214417 (2009), arXiv:0901.4498.

³⁰ R. Valentí, T. Saha-Dasgupta, and F. Mila, *Phys. Rev. B*, **68**, 024411 (2003), cond-mat/0209515.

³¹ The fit is complicated by the substantial hybridization between V $3d$ and Cd $5s$ states. Since the ambiguity of the fit could affect the hopping parameters and thus the resulting exchange integrals, we carefully tested our estimates by varying energy windows for Wannier functions or adding

- explicit contributions of Cd 5s orbitals as “tails”. We also constructed a 24-band model including Wannier functions with Cd 5s character. All these tests produced rather similar results and confirmed our main conclusion on the FM superexchange in CdVO₃.
- ³² H. Eschrig and K. Koepnik, Phys. Rev. B, **80**, 104503 (2009), arXiv:0905.4844.
 - ³³ A. A. Tsirlin, R. Nath, J. Sichelschmidt, Y. Skourski, C. Geibel, and H. Rosner, (2011), arXiv:1101.2546.
 - ³⁴ A. A. Tsirlin and H. Rosner, Phys. Rev. B, **83**, 064415 (2011), arXiv:1011.3981.
 - ³⁵ K. I. Kugel and D. I. Khomskii, Sov. Phys. Usp., **25**, 231 (1982).
 - ³⁶ V. V. Mazurenko, F. Mila, and V. I. Anisimov, Phys. Rev. B, **73**, 014418 (2006), cond-mat/0509315.
 - ³⁷ A. A. Tsirlin, O. Janson, and H. Rosner, Phys. Rev. B, **82**, 144416 (2010), arXiv:1007.1646, and references therein.
 - ³⁸ A. A. Tsirlin, A. A. Belik, R. V. Shpanchenko, E. V. Antipov, E. Takayama-Muromachi, and H. Rosner, Phys. Rev. B, **77**, 092402 (2008), arXiv:0801.1434.
 - ³⁹ For example: R. Zinke, S.-L. Drechsler, and J. Richter, Phys. Rev. B, **79**, 094425 (2009), arXiv:0807.3431.
 - ⁴⁰ E. R. Ylvisaker, W. E. Pickett, and K. Koepnik, Phys. Rev. B, **79**, 035103 (2009), arXiv:0808.1706, and references therein.
 - ⁴¹ A. A. Tsirlin, I. Rousochatzakis, D. Kasinathan, O. Janson, R. Nath, F. Weickert, C. Geibel, A. M. Läuchli, and H. Rosner, Phys. Rev. B, **82**, 144426 (2010), arXiv:1008.1771.
 - ⁴² J. Choukroun, V. A. Pashchenko, Y. Ksari, J. Y. Henry, F. Mila, P. Millet, P. Monod, A. Stepanov, J. Dumas, and R. Buder, Eur. Phys. J. B, **14**, 655 (2000).
 - ⁴³ V. A. Pashchenko, A. Sulpice, F. Mila, P. Millet, A. Stepanov, and P. Wyder, Eur. Phys. J. B, **21**, 473 (2001), cond-mat/0103441.
 - ⁴⁴ D. Aldous, R. J. Goff, J. P. Attfield, and P. Lightfoot, Inorg. Chem., **46**, 1277 (2007).
 - ⁴⁵ C. Weeks, Y. Song, M. Suzuki, N. A. Chernova, P. Y. Zavalij, and M. S. Whittingham, J. Mater. Chem., **13**, 1420 (2003).
 - ⁴⁶ I. Chaplygin, R. Hayn, and K. Koepnik, Phys. Rev. B, **60**, R12557 (1999), cond-mat/9906385.
 - ⁴⁷ I. Chaplygin and R. Hayn, Phys. Rev. B, **70**, 064510 (2004).
 - ⁴⁸ H.-J. Koo and M.-H. Whangbo, Solid State Sci., **12**, 685 (2010).
 - ⁴⁹ Here, we use $U_d = 3$ eV for five-fold-coordinated V⁺⁴ (MgVO₃, VOSb₂O₄), $U_d = 4$ eV for six-fold-coordinated V⁺⁴ (Ba₂V₃O₉, CsVOF₃, VO(ac)₂), and $J_d = 1$ eV for all test compounds. The octahedral oxygen environment requires a higher U_d , as shown in, e.g., Refs. 26 and 29.
 - ⁵⁰ To reach the experimental Curie temperature, one has to take $J_a/J_1 = 0.07$ which is, however, inconsistent with the susceptibility fit. Since there are four couplings J_a and two coupling J_c at each lattice site, $J_a/J_1 = 0.07$ increases the overall energy of the interchain couplings by 70 %, and alters the susceptibility fit.
 - ⁵¹ For example: V. Gnezdilov, P. Lemmens, A. A. Zvyagin, V. O. Chervanovskii, K. Lamonova, Y. G. Pashkevich, R. K. Kremer, and H. Berger, Phys. Rev. B, **78**, 184407 (2008), arXiv:0810.0679.
 - ⁵² M. E. Fisher, Amer. J. Phys., **32**, 343 (1964).
 - ⁵³ A. W. Sandvik, Phys. Rev. Lett., **83**, 3069 (1999), cond-mat/9904218.
 - ⁵⁴ P. Sengupta, C. D. Batista, R. D. McDonald, S. Cox, J. Singleton, L. Huang, T. P. Papageorgiou, O. Ignatchik, T. Herrmannsdörfer, J. L. Manson, J. A. Schlueter, K. A. Funk, and J. Wosnitza, Phys. Rev. B, **79**, 060409(R) (2009).
 - ⁵⁵ O. Janson, J. Richter, P. Sindzingre, and H. Rosner, Phys. Rev. B, **82**, 104434 (2010), arXiv:1004.2185.
 - ⁵⁶ A. A. Tsirlin and H. Rosner, Phys. Rev. B, **82**, 060409(R) (2010), arXiv:0910.2056.
 - ⁵⁷ To verify the role of Pb in PbVO₃, we evaluated the second-neighbor coupling J_2 in the fictitious SrVO₃ having the tetragonal PbVO₃ structure. The calculations yield $J_2 = 24$ K in SrVO₃ against $J_2 = 69$ K in PbVO₃.
 - ⁵⁸ A. A. Tsirlin, R. V. Shpanchenko, E. V. Antipov, C. Bougerol, J. Hadermann, G. Van Tendeloo, W. Schnelle, and H. Rosner, Phys. Rev. B, **76**, 104429 (2007), arXiv:0710.1806.
 - ⁵⁹ W. Geertsma and D. Khomskii, Phys. Rev. B, **54**, 3011 (1996).
 - ⁶⁰ K. Kopinga, T. Delica, and H. Leschke, Phys. Rev. B, **40**, 7239 (1989); L. S. Campana, A. Caramico D’Auria, U. Esposito, and G. Kamieniarz, **41**, 6733 (1990); K. Kopinga, T. Delica, H. Leschke, and I. Riedel, **47**, 5447 (1993).
 - ⁶¹ K. Kopinga, A. M. C. Tinus, W. J. M. de Jonge, and G. C. de Vries, Phys. Rev. B, **36**, 5398 (1987); G. C. de Vries, E. Frikkie, K. Kakurai, M. Steiner, B. Dorner, K. Kopinga, and W. J. M. de Jonge, **40**, 7011 (1989).